LES of cylinder plate configurations and corresponding aeroacoustic effects

M. KORNHAAS[a], M. WINKLER[b], D.C. STERNEL[a], K. BECKER[b], M. SCHÄFER[a], F. KAMEIER[c]

a. Technische Universität Darms tadt, Chair of Numerical Methods in Mechanical Engineering, Dolivostraße 15, 64289 Darmstadt, Germany
b. Cologne University of Applied Sciences, Institute of Automotive Engineering, Betzdorfer Straße 2, 50679 Cologne, Germany
c. Düsseldorf University of Applied Sciences, Fachbereich Maschinenbau und Verfahrenstechnik, Josef-Gockeln-Straße 9, 40474 Düsseldorf, Germany

Abstract :

Large Eddy Simulations together with experimental investigations of an aeroacoustic test case consisting of a plate located in the turbulent wake of a circular cylinder are presented. The investigations focus on the frequency changes due to variations of the test case geometry and the ability of the numerical method to capture these phenomena.

Mots clefs : LES, Cylinder Plate Configuration, Aeroacoustic

1 Introduction

A great part of the noise in our daily life is generated by turbulent flows, e.g. the noise of driving cars or fans. Even though the prediction and reduction of noise is an important issue, the physical mechanisms of noise generation in turbulent flows are still not fully understood. Computational fluid dynamics (CFD) can be a very useful tool to give a deeper insight into the flow physics since it allows a more detailed view on flow features than experiments. However, only recently sufficient computational power has become available for the predictive simulation of turbulent flows for more complex geometries and higher Reynolds numbers, since in many cases only time resolved simulations like the Direct Numerical Simulation (DNS) or the Large Eddy Simulation (LES) can provide reliable results.
Both techniques the DNS - where the Navier-Stokes equations are solved directly and all time and length scales have to be resolved - and the LES - where the turbulent motions of the grid scale are calculated directly and only the subgrid scales are modeled - require a high resolution in space and time and are therefore highly time- and resource-consuming.
We present LES results of the flow field around a cylinder plate configuration as well as experimental data of the sound pressure spectrum for this test case. The test case consists of a plate which is located in the turbulent wake of a circular cylinder. The geometrical simplicity of the configuration in combination with an enormous superelevation of the sound pressure at low flow speeds by adding a simple plate makes this test case very attractive for the validation for low Mach number aeroacoustic codes.
Experimental investigations show a high sensitivity of the frequency spectrum of the acoustic pressure to changes of the distance between plate and cylinder as well as to an offset of the plate to the cylinder axis. The aim of this study is to prove if the applied numerical method is capable to reproduce those effects on the dominant frequencies in the flow field and therefore its capability for further aeroacoustic studies.

2 Test case description

The investigated configuration consists of a steel plate which is located in the turbulent wake of a circular cylinder (compare figure 1). The Reynolds number based on the diameter D of the cylinder and the free stream velocity is around $Re_D = 2000$.

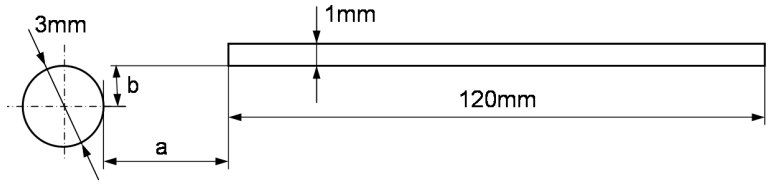

FIG. 1 – Test case configuration.

3 Experimental investigations

The experimental investigations were carried out at NVH.Lab at Cologne University of Applied Sciences. Sound pressure spectra are measured and the sensitivity to geometrical changes is investigated.
Figure 2 shows the experimental setup as well as the acoustic sound pressure spectrum for the test case configuration and a single cylinder. A significant increase of the sound pressure level compared to the single cylinder can be observed. Further the dominant frequency is lower for the test case compared to the single cylinder. By decreasing the distance a between plate and cylinder at a constant offset $b = 1.5$ mm (compare figure 1)

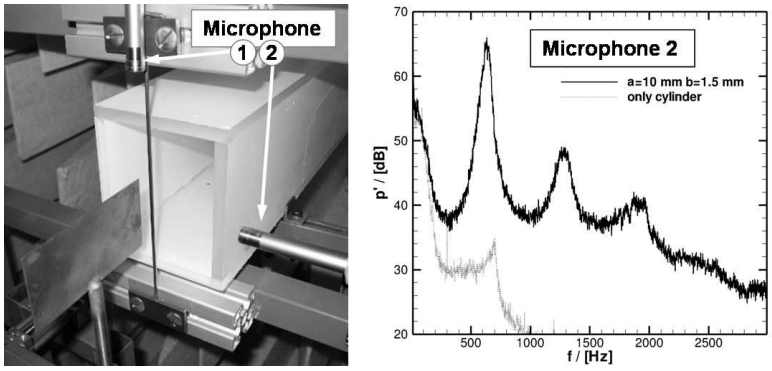

FIG. 2 – Experimental setup (left) and sound pressure spectrum for the test case and a single cylinder (right).

an increase of the dominant frequency can be observed (figure 3, left). Whereas if the plate is in line with the cylinder (offset $b = 0$) a shift towards lower frequencies takes place (figure 3, right). For both considered offsets b the sound pressure level is lower if the plate is located closer to the cylinder.

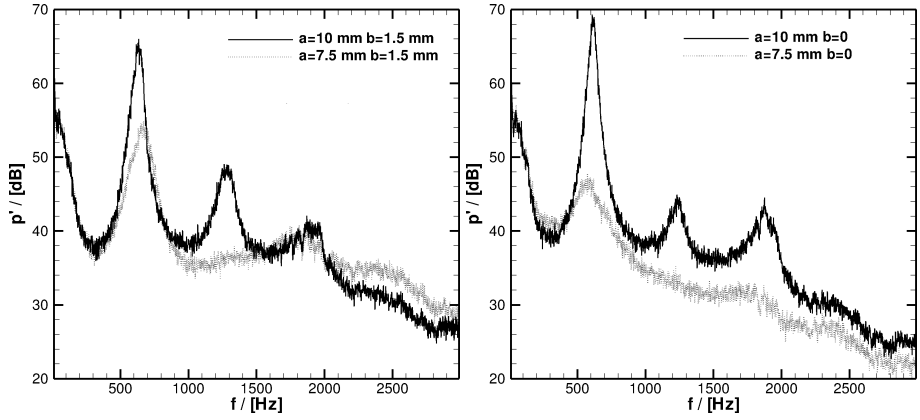

FIG. 3 – Measured sound pressure spectra for different geometric configurations.

4 Numerical setup

4.1 Numerical method and code description

LES are performed utilizing the incompressible finite volume solver FASTEST [1]. The filtered *Navier-Stokes* equations are solved on boundary fitted, block structured hexahedral grids. Convective and diffusive fluxes are

approximated with a second-order central difference scheme. Subgrid stresses are computed using the Smagorinsky model with the dynamic approach of Germano [2]. The implicit second order Crank-Nicolson scheme is applied for time discretization. Pressure velocity coupling is realized with a SIMPLE type algorithm which is embedded in a geometric multi-grid scheme with standard restriction and prolongation [3]. The resulting linear systems of equations are solved with an ILU method.

4.2 Acoustic source term modeling

Time resolved computations of the flow field like LES allow the calculation of aeroacoustic sources according to different aeroacoustic analogies like Lighthill's analogy [4] or Hardin and Pope's [5] acoustic/viscous splitting approach. In the latter the compressible flow field at low Mach numbers is modeled as an incompressible calculated hydrodynamic part (denoted with $*^{inc}$) and an acoustic fluctuation (denoted with $*'$). In the following $\vec{u}$ stands for the velocity vector, p for the pressure, ρ for the density and κ for the adiabatic exponent. Further the hydrodynamic density correction $\rho^{(1)}$ is introduced. If viscous effects are neglected, this approach leads to a system of equations which is equivalent to the *Linearized Euler Equations* (LEE) on the left hand side and acoustic sources on the right hand side,

$$\frac{\partial \rho'}{\partial t} + \rho^{inc}\nabla \cdot \vec{u}' + \vec{u}^{inc} \cdot \nabla \rho' = -\frac{\partial \rho^{(1)}}{\partial t} - \vec{u}^{inc} \cdot \nabla \rho^{(1)} \tag{1}$$

$$\rho^{inc}\frac{\partial \vec{u}'}{\partial t} + \rho^{inc}\left(\vec{u}^{inc} \cdot \nabla\right)\vec{u}' + \nabla p' = 0 \tag{2}$$

$$\frac{\partial p'}{\partial t} + \kappa p^{inc}\nabla \cdot \vec{u}' + \vec{u}^{inc} \cdot \nabla p' = -\frac{\partial p^{inc}}{\partial t} - \vec{u}^{inc} \cdot \nabla p^{inc} \tag{3}$$

with the hydrodynamic density correction

$$\rho^{(1)} = \frac{p^{(1)}}{c_\infty} = \frac{1}{c_\infty}\left(p^{inc} - \lim_{T\to\infty}\int_0^T p^{inc} dt\right) = \frac{1}{c_\infty}\left(p^{inc} - <p^{inc}>\right) \tag{4}$$

where c_∞ stands for the speed of sound and $<p^{inc}>$ for the mean hydrodynamic pressure. According to this approach for interpretation of the flow field with respect to noise generation mechanisms we focus on the incompressible pressure fluctuations that are the dominant part in the source term for the acoustic pressure fluctuation p'.

4.3 Numerical setup

The computational domain is modeled periodically in spanwise directions. The inlet velocity is set to 10m/s corresponding to the desired Reynolds number of approximately $Re_D = 2000$. All walls are no slip walls and zero gradient boundary conditions are applied at the outlet.
In order to minimize disturbances of the flow caused by boundary conditions - the size of the computational domain was chosen sufficiently big. It is of the size 100 D in streamwise direction. Hereby the inlet is located 15 D upstream the cylinder. In spanwise directions 5 D respectively 50 D are modeled.
The boundary layer around the cylinder is fully resolved with corresponding y^+ values of the order $\mathcal{O}(1)$ whereas the developing boundary layer attached to the plate is not resolved. The resulting grid consist of approximately 2.47×10^6 control volumes. The grid structure is displayed in figure 4 .
The time step size was set to 1.6×10^{-6}s which results in Courant numbers below unity. The simulations were set up on 8 IBM Power5 CPUs with a load balancing efficiency of 98.5%. This leads to computational times of approximately 12 seconds per time step. Turbulence statistics were performed for at least 16000 time steps.

4.3.1 Performed simulations

Four simulations of the cylinder plate configuration with varied distances $a = 7.5$ mm and $a = 10$ mm and the offsets $b = 1.5$ mm and $b = 0$ (compare figure 1) were carried out in order to prove the ability of the numerical method to reproduce the changes of the frequencies described in section 3.
Another computation of a single cylinder at the same Reynolds number was carried out in order to compare the pressure fluctuations that are a measure for the emitted sound pressure level.

5 Results

In the following a selection of results is presented. We focus on the configuration with the offset $b = 1.5$ mm and vary the cylinder plate distance a (compare figure 1).

5.1 Flow features

To give an impression of the turbulent structures around the test case the vorticity magnitude is shown in figure 4. It is obvious that the *von Karman vortex street* can not develop if the plate is present. The interaction of

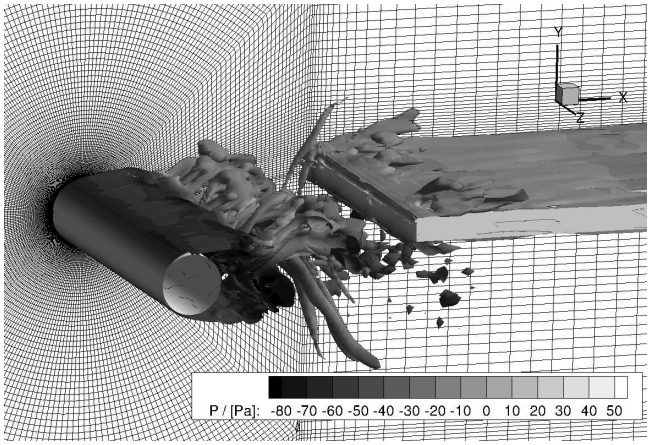

FIG. 4 – Grid structure and vortical structures in the vicinity of the test case - snapshot of the vorticity magnitude colored by pressure.

the vortex shedding at the cylinder with the front edge of the plate leads to high time dependent pressure fluctuations and therefore high aeroacoustic sources. In figure 5 the pressure distribution for two different time steps is shown in oder to illustrate this behavior. The mean pressure fluctuations $<p^{'inc}>$ for the configuration

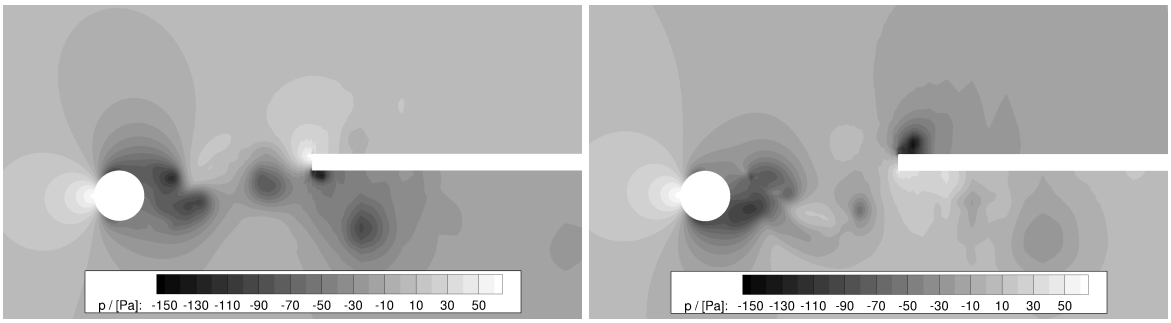

FIG. 5 – Unsteady pressure distribution at two different time steps (time between snapshots : $8 \cdot 10^{-4}$s).

with $a = 10$ mm, $b = 1.5$ mm and those obtained for a single cylinder at the same Reynolds number are shown in figure 6. The absolute values of the pressure fluctuations are up to 5 times larger for the test case compared to the single cylinder what also gives an explanation of the significantly higher level of emitted noise observed in the experiments (compare figure 2).

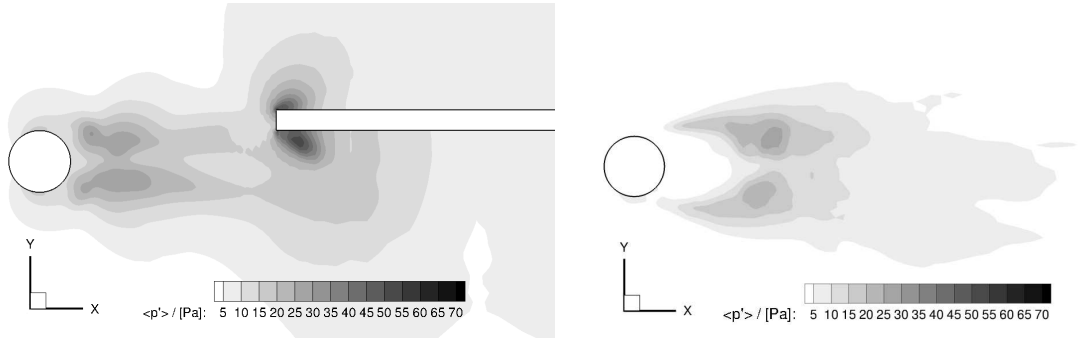

FIG. 6 – Mean pressure fluctuations for the test case (left, $a = 10$ mm, $b = 1.5$ mm) and a single cylinder (right).

5.2 Frequency spectra

To get information about the frequencies on which the sound is emitted and to identify the corresponding flow features, time series were recorded at different monitoring locations. The locations of the monitoring points (MP) are depicted in figure 7. Since the highest pressure fluctuations occur at the front edge of the plate and

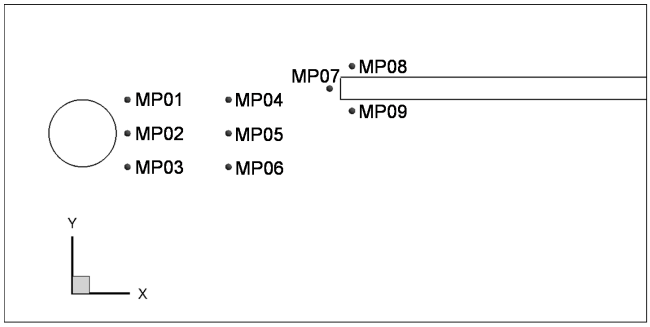

FIG. 7 – Location of the monitoring points (MP).

therefore the dominant acoustic sources can be expected in this region we focus on MP09 in the following. MP09 is located 0.5 mm behind the front edge of the plate and 0.5 mm below it.
Figure 8 (left) shows the frequency spectrum of the simulated incompressible pressure for the configurations with $a = 10$ mm and $a = 7.5$ mm and the offset $b = 1.5$ mm. For the case $a = 10$ mm the peaks that are present in the measured sound pressure spectrum can also be identified in the simulations whereas for $a = 7.5$ mm the first harmonic is present in the simulation but not in the measured spectrum. It can be stated that these phenomena can not be explained by the pressure spectrum alone. Also the shift towards a higher frequency for smaller a as seen in the experiments can not be reproduced, actually the opposite trend is present in the simulations. Further no conclusion can be drawn from the pressure spectrum to the different levels of emitted noise for the two considered distances a.
In figure 8 (right) the spectrum of $\frac{\partial p^{inc}}{\partial t}$ as dominant part of the aeroacoustic source term is displayed. In contrast to the pressure spectrum a significant difference for the two considered cylinder plate distances is present. For $a = 10$ mm the overall level in the $\frac{\partial p^{inc}}{\partial t}$ spectrum is higher especially the second peak that is equivalent to the first harmonic is much more distinct. The higher sound pressure level for the larger distance a may be explained by this as well as the absence of the first harmonic in the sound pressure spectrum for $a = 7.5$ mm. As for the pressure spectrum the trend towards a higher frequency for the smaller a can not be observed.

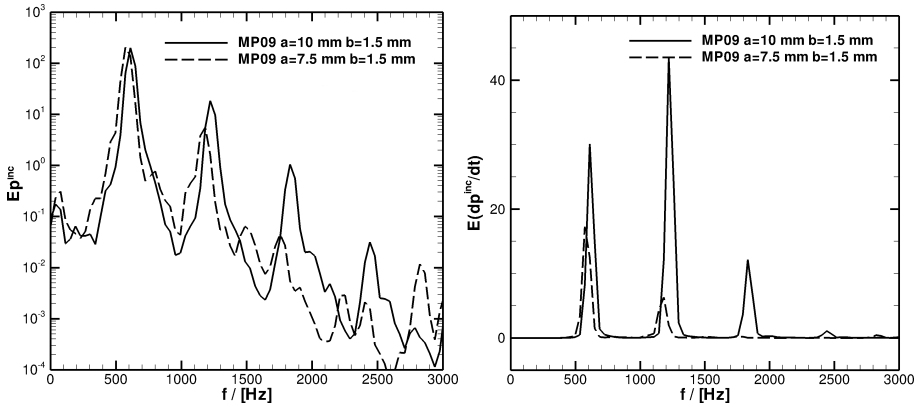

FIG. 8 – Frequency spectra of pressure (left) and $\frac{\partial p^{inc}}{\partial t}$ (right) for the configurations with $b = 1.5$ mm and varied a.

Table 1 shows the experimentally and numerically obtained frequencies. For the greater cylinder plate distance $a = 10$ mm a good agreement with the experiments can be stated whereas for the smaller distance the deviation is of approximately 15%. The question if the quality of the simulation is the reason for this deviation or if solely acoustic effects – like the interaction of acoustic waves, etc. – are the cause for the changes of the dominant frequency in the sound pressure spectrum are on the focus of ongoing investigations.

TAB. 1 – Numerically obtained frequencies in comparison to experimental values.

Configuration	f / [Hz] - Experiment	f / [Hz] - Simulation	Deviation %
$a = 10$ mm, $b = 1.5$ mm	634	610	3.8
$a = 7.5$ mm, $b = 1.5$ mm	669	569	15.0

6 Conclusion

An aeroacoustic test case consisting of a plate located in the turbulent wake of a circular cylinder was introduced. Further a selection of experimental results as well as numerical results obtained by LES were presented. In our presentation we will give a more detailed view on the applied numerical methods and we will present results for all measured geometry variations together with an appropriate discussion of the results.
Further we will present the simulated acoustic field for the test case and corresponding acoustic sound pressure spectra that are subject of ongoing investigations.

7 Acknowledgement

This work was partially supported by the DFG within the collaborative research center “Flow and Combustion in future Gas Turbine Combustion Chambers”, SFB 568 and the French-German research unit 507, “LES of complex flows” as well as by the competence platform, “Sound and Vibration Engineering”, sponsored by the MIWFT of the federal state of North Rhine-Westphalia, Germany.

Références

[1] Fastest manual. Chair of Numerical Methods in Mechanical Engineering, Technische Universität Darmstadt, Germany, 2005.

[2] Germano M., Piomelli U., Moin P., and Cabot W. H. A dynamic subgrid-scale eddy viscosity model. Phys. of Fluids A, 3, 1760–1765, 1991.

[3] Briggs W. L., Henson V. E., and McCormick S. F. A multigrid tutorial, SIAM 2000.

[4] Lighthill M. On sound generated aerodynamically 1 : General theory. Proc. Roy. Soc. London Series A, 211, 654–857, 1952.

[5] Hardin J. and Pope D. An acoustic/visous splitting technique for computational aeroacoustics. Theoret. Comp. Fluid Dynamics, 6, 323–340, 1994.